Development of a Rapid-Response Flow-Control System Using MEMS Microvalve Arrays

John Collier, Donald Wroblewski, and Thomas Bifano

***Abstract*—A method for providing high-resolution gas flow control using microelectromechanical systems (MEMS) has been developed and tested. The micromachined component consists of an array of 61 synchronized microvalves operating in parallel. A number of tests were conducted on microvalves of various designs to characterize their operation. The best performing of these was used with a prototype flow controller. Additionally, a mathematical model of the flow system and controller was derived to predict the response of the system to various changes in operating conditions. This paper describes the design, modeling, and testing of a compact, stand-alone mass flow controller (MFC) to demonstrate high resolution, fast response flow control using MEMS microvalves. The device consists of a microvalve array packaged with a micro flow sensor and a microprocessor-based control system. The high bandwidth of microvalves allows an atypical flow control architecture. The controller regulates a pulsewidth-modulated (PWM) signal sent to the valve array and is capable of both open- and closed-loop control. A mathematical model was also developed to predict the dynamic performance of the system under various operating conditions. Additional advantages of the MEMS flow-control system include low-power consumption, low fabrication costs, and scalable precision. [1119]**

***Index Terms*—Closed-loop systems, fluid flow control, microelectromechanical devices, pulsewidth modulation (PWM), valves.**

I. Introduction

THE primary motivation of this paper is to evaluate the performance of microelectromechanical systems (MEMS) microvalve arrays (μvalves) used as gas flow control devices. This led to the development of an apparatus which, when combined with a μvalve, would comprise a robust mass flow control system. It will be shown that the μvalve flow controller exhibits fine resolution, wide flow range, and fast response.

Early generations of the μvalve devices were previously reported by Vandelli [1], [2]. Hodge [3], [4] incorporated improved μvalves into a flow system and conducted a number of experiments to evaluate their performance. A single microvalve is composed of a thin film silicon plate anchored along two opposite edges. The plate is fabricated using surface-micromachining processes and is positioned several micrometers over a bulk-micromachined orifice extending through the substrate. Electrostatic attraction is used to deflect the plate and seal off the corresponding hole. The valves operate in a binary fashion; each microvalve is either fully open or fully closed.

Manuscript received July 21, 2003; revised April 5, 2004. Subject Editor G. B. Hocker.

The authors are with the Precision Engineering Research Lab, College of Engineering, Boston University, Boston, MA 02215 USA (e-mail: bifano@bu.edu).

Digital Object Identifier 10.1109/JMEMS.2004.838392

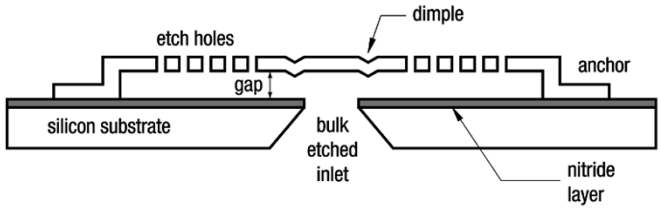

Fig. 1. Microvalve cross section. Note that the gap height dimension is exaggerated for clarity.

A cross-sectional view of a single microvalve is shown in Fig. 1. The device consists of a polysilicon plate anchored over a hole in a silicon substrate. The plate is separated from the substrate by a 2 μm gap. Plate sizes vary from 300 to 400 μm. Gas flow enters the device through the substrate inlet (250 μm square) and exits through the sides of the valve (perpendicular to the page in Fig. 1) and through the etch holes. The valve is closed using electrostatic attraction; applying an appropriate voltage to the plate, with the substrate grounded, causes it to deflect downward and seal the hole. A thin layer of silicon nitride between the plate and the substrate prevents direct contact during actuation (which would cause a short circuit). A polysilicon routing wire on the substrate connects the valve plate to a peripheral pad near the edge of the chip, where it can be attached to external driver circuitry.

When the valve actuates, the electrostatic force increases quadratically as the gap decreases. If the actuation voltage is not sufficient to close the valve, an equilibrium exists between the electrostatic applied force and the mechanical restoring force acting on the plate. When the voltage is increased to a critical point, however, the electrostatic force overcomes the restoring force. This causes the center of the plate to collapse against the substrate, sealing the hole. This phenomenon is known as snap-through, and the critical voltage is referred to as the snap-through voltage.

Given the small dimensions of the gap, blockage of the valves by particulate matter could pose problems. However, use of filters upstream of the valves has proven to be highly effective in mitigating this effect, as evidenced by the repeatability of flow versus pressure curves and the lack of evidence of fouling in visual inspection of valves.

The mechanical and fluidic design approach for the valves has been reported by Vandelli [1], [2]. Based on characterizations of different valve types by Hodge [3], [4], the μvalve actuator design for this paper was chosen to be a plate fixed along two edges (designated as double-cantilever or "DC" in subsequent illustrations), with three different plate sizes: 300, 400, and 500 μm. Fig. 2 displays the size variations of the design.

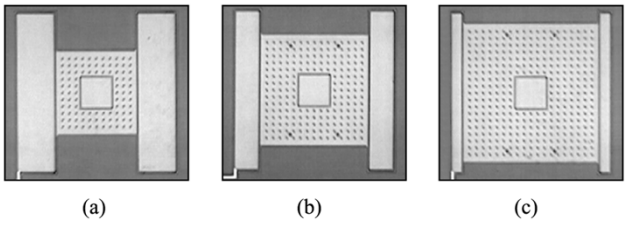

Fig. 2. Optical microscope photos of various sizes of double-cantilever valve (with dimples). (a) 300 μm. (b) 400 μm. (c) 500 μm.

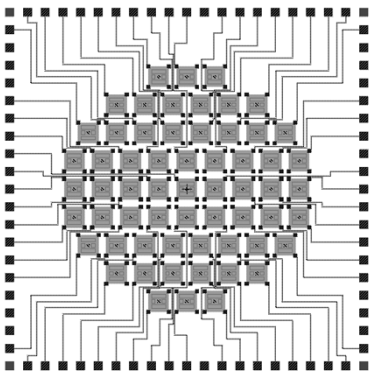

Fig. 3. Layout of 61-Valve Array.

Additionally, actuator plates were made both with and without a dimpled area around the center of the plate; this was intended to prevent stiction (a condition where the valve plate does not immediately release when power is removed).

The valves were arranged in an array of 61 on a 1 cm^2 chip (Fig. 3). The valve arrays were manufactured for Boston University by Cronos Integrated Microsystems, and the fabrication process was detailed by Vandelli [1], [2]. Prior to testing, the arrays were mounted and wire-bonded to a ceramic chip carrier.

To take advantage of the valves high speed response, pulsewidth modulation (PWM) was used for control. PWM involves actuating the microvalves with a high frequency square wave and varying the duty cycle to regulate flow rate. The use of PWM for fluid flow control is not unique. PWM is commonly used for atomizers and with solenoid control valves, since it provides a means for a highly linear way to control flow with a constant inlet pressure. However, these types of systems utilize PWM for open loop control (not closed loop), and in many cases the overall response rates are limited by the valve response times. The unique aspect of the system reported here is the use of PWM combined with ultrafast microvalves (actuation times on the order of 10 μs) for closed loop control to provide for high dynamic range and precision with fast response times.

II. System Development

A. Valve Characterization

A number of tests were conducted to investigate such factors as flow rate and pressure capability, leakage, and response time.

The ideal valve would combine such qualities as low snap-through voltage, high flow rate, low propensity for stiction, low leakage rate, and the capability of high pressure operation. Some performance attributes can be optimized by

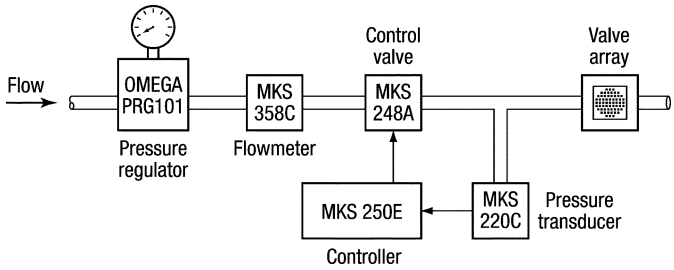

Fig. 4. Layout of microvalve testing apparatus.

modifying certain valve dimensions, but more often, competing effects require a design trade-off. For example, stiction can be reduced by stiffening the valve plate and thus increasing the mechanical restoring force. However, this results in a higher snap-through voltage. (Minimizing the actuation voltage is advantageous because it allows for more compact and economical electronics.)

The 300-μm size proved difficult to actuate, even under application of high voltages ($\sim$150 V), and was therefore eliminated from testing.

The remaining valve sizes (400 and 500 μm) were tested to evaluate two of the most important valve characteristics—flow rate and snap-through voltage. Compressed air (Medical Air USP) was used in all tests and the valve pressure was controlled using a pressure control system from MKS Instruments (consisting of a Model 220C Pressure Gauge, a Model 248A Control Valve, and a Model 250E Pressure/Flow Controller). Flow rate measurements were obtained with a Model 358C Mass Flow Meter. The upstream pressure of the system was preregulated using an OMEGA PRG101-25 pressure regulator. Fig. 4 displays a schematic of the test apparatus. Single valve chips, not arrays, were used in these tests. Since the range of the mass flow meter is only 50 sccm (standard cubic centimeters per minute), the use of single valves allowed the flow rate versus pressure relationship to be investigated at higher pressures. For each valve under test, the flow rate was measured at varying pressures, with the valve actuated at each step to verify closure. Pressure was increased until the device failed or would no longer actuate.

Fig. 5 presents flow rate versus pressure results for unenergized valves with and without dimples. Each valve was tested to failure, and it can be seen that valves with dimple reinforcements were able to withstand higher pressure than those without. Fig. 6 presents the voltage required for closing the valves as a function of pressure. The data show, as expected, that valves actuating against increased differential pressure require increased voltage to induce snap-through. The higher actuation potential has a negative effect on valve reliability. After snap-through occurs, higher voltages cause the valve to be susceptible to short circuits with the grounded substrate in the region around the through-hole. The placement of dimples around the center of the plate, however, stiffens the valve and supports it in this critical region near the hole, reducing the chance of failure. Thus, valves with dimples were operable to higher pressures.

Flow leakage—small amounts of gas passing through a closed valve—was observed in all valves tested. This is likely due to the imperfect seal formed between the substrate and the dimples As will be shown, the leakage limits the maximum

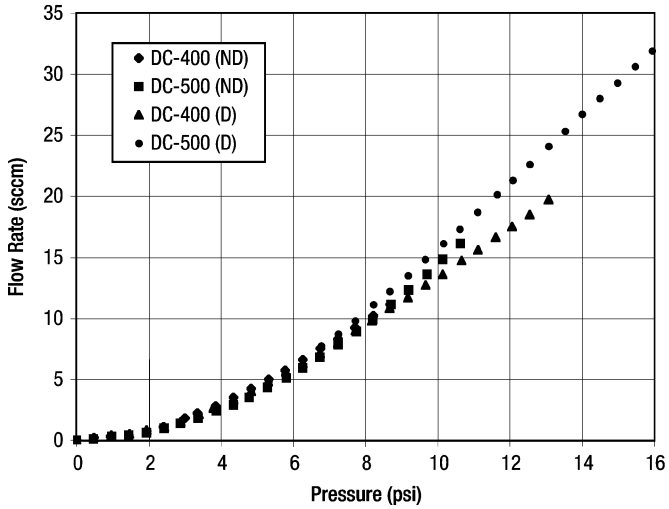

Fig. 5. Measured flow versus pressure results for single valves with dimples (D) and without dimples (ND).

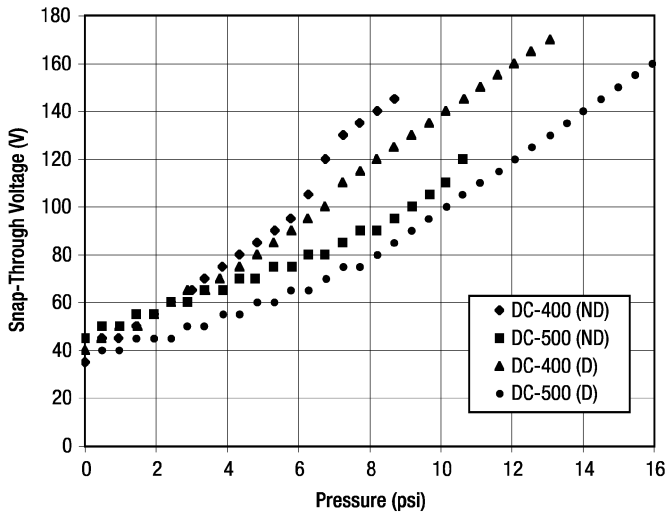

Fig. 6. Snap-through voltage versus pressure measurements for single valves with dimples (D) and without dimples (ND).

obtainable dynamic range. Experiments were performed in which the valve was operated using a reverse-flow configuration in an attempt to reduce leakage. In this arrangement, fluid flows first through the actuator plate gap and then out through the substrate port. The pressure differential acts to assist electrostatic actuation forces on the membrane, rather than to oppose them. This configuration should, in principal, decrease the leakage rate. This hypothesis was tested using a 400-μm double-cantilever valve with dimples, and the leakage results are shown in Fig. 7. It is clear from this plot that reversing the direction of flow does in fact reduce the leakage rate. However, it comes at the expense of significantly reduced flow rate when the valve is open. Pressure versus flow tests for the DC-400 valve indicated that a pressure differential of approximately 7 psi was sufficient to force the valve completely shut in the reverse-flow configuration, absent any electrostatic actuation. Even at lower pressures, the flow was significantly restricted, compared to forward operation, by a factor of 5 to 10.

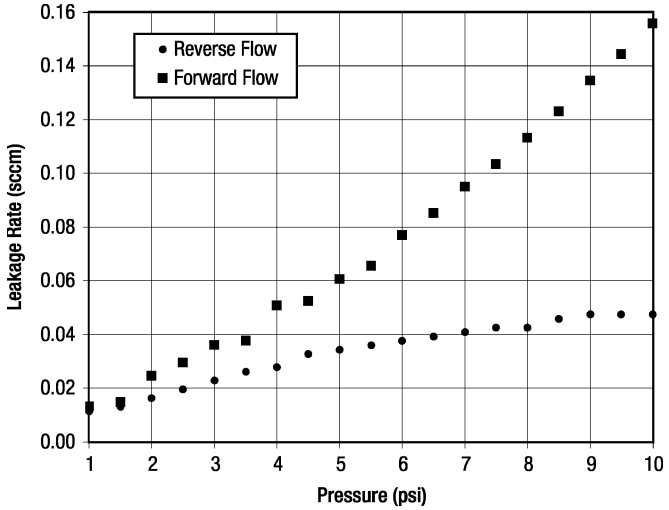

Fig. 7. Leakage rate versus pressure of DC-400 single valve (with dimples). Flow in reverse and forward directions.

The dynamics of microvalve actuation were investigated. As will be shown later, these dynamics play a significant role in the performance of the flow control system. Measurements with a laser vibrometer indicated a valve closing time (with no pressure differential across the valve) of $\sim$58 μs, and a valve opening time of $\sim$10 μs. The time required for closing is dominated by the dynamics of the drive electronics for the actuator, whereas the time required for opening is dominated by the mechanical dynamics of the valve itself.

B. Valve Actuation

To take advantage of the μvalves' exceptionally high speed (14 kHz), a PWM actuation scheme was used. This method involves connecting all the valves of an array together so they operate synchronously, then driving them with a square wave. The flow rate is varied by adjusting the duty cycle of the square wave. The duty cycle is defined as

$$\mathrm{DC} = \frac{t_{\mathrm{on}}}{T} \tag{1}$$

where T is the period of the wave and t_{on} is the high time of the period, as shown in Fig. 8. Ideally, PWM actuation provides a flow rate equal to

$$Q = Q_{\mathrm{FS}}(1 - \mathrm{DC}) \tag{2}$$

where Q_{FS} is the full-scale flow rate (at 0% duty cycle).

The PWM technique provides a high degree of linearity over most of the flow range. Additionally, it allows for very high resolution. A change in duty cycle, no matter how small, will produce a proportional change in flow rate. This effectively allows the controller to exploit the inherently fast response time of the valves to achieve very high precision. The PWM method also provides scalability for the valve array, meaning that the number of valves can be increased or decreased without a significant detriment to performance, and without the need for large numbers of electrical leads and connections.

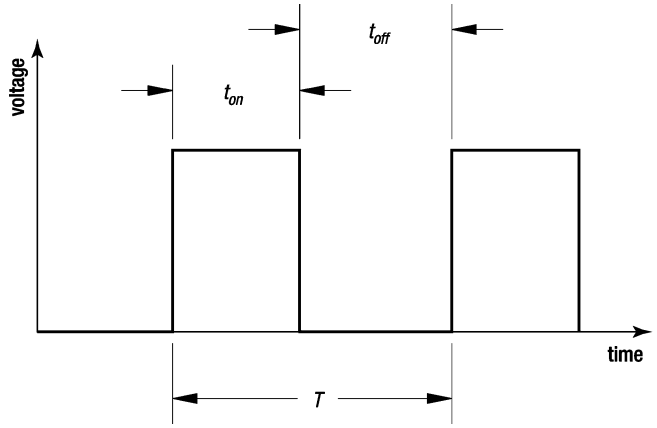

Fig. 8. Representation of PWM.

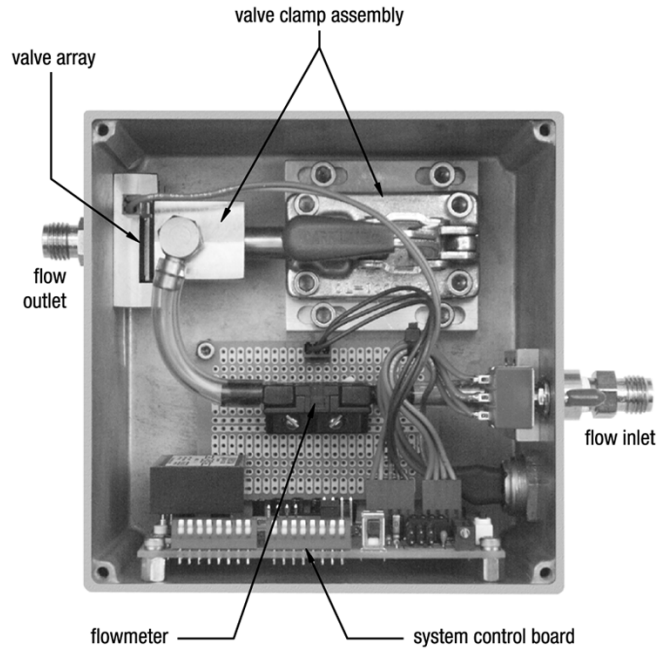

Fig. 9. Interior view of MFC.

C. Mass Flow Controller (MFC)

A system was developed to use the MEMS microvalves to provide high-resolution gas flow control. The layout of components used in the MFC can be seen in Fig. 9. The gas to be controlled is connected to the inlet and passes through a flowmeter before reaching the microvalve array. Both the flowmeter and valve array are monitored by the microcontroller on the system control board.

The valve array chip carrier is placed in a stainless steel fixture and held in place with a toggle clamp. The clamp is mounted on a moveable plate which allows the clamping force to be adjusted. A Honeywell AWM3150V was chosen as the mass airflow sensor. This device features a fast, linear response, which simplifies the control software.

The system is controlled by a custom-designed circuit including a Motorola HC12 microcontroller, a high-voltage power supply, and a high-speed analog amplifier.

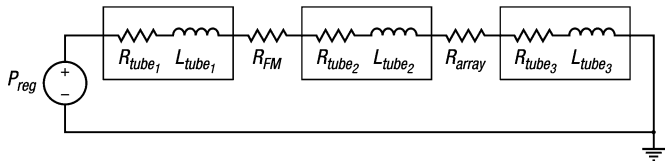

Fig. 10. Electric circuit representation of flow system.

III. Mathematical Modeling

The use of both open- and closed-loop control systems called for the development of a mathematical representation of the MFC. This allows prediction of the system's dynamic response to changes in user setpoint or input pressure. Additionally, parameters of the closed-loop controller could be optimized using the model, resulting in improved performance.

A. Model Development

Modeling the system as a whole requires determination of the time constants of the individual components. These include the pressure regulator, flowmeter, microvalves, and the fluidic response. The latter is of particular interest because it is difficult to determine experimentally.

The fluidic component of the model, in this case, refers to fluidic resistance and inertance effects due to the flow path through the microvalves and through tubing and fittings in the system. The system to be modeled is shown in Fig. 10. It begins at the pressure regulator, modeled as a constant pressure source. The flow passes through a length of tubing to the flowmeter, then through another tube to the valve array, and finally, through another tube where it is vented to the atmosphere. Each tube length is modeled as a resistance in series with an inductance, and the flowmeter and valve array are each represented as single resistances.

The differential equation describing the system is

$$P_{\text{reg}} = (R_{\text{tube}_1} + R_{\text{tube}_2} + R_{\text{tube}_3} + R_{\text{flowmeter}} + R_{\text{array}})\,Q + (L_{\text{tube}_1} + L_{\text{tube}_2} + L_{\text{tube}_3})\,\dot{Q} \quad (3)$$

where Q represents the flow rate (i.e., current) of the system, and R and L represent fluid resistance and inertance components, respectively.

To account for excluded items such as fittings and tube bends, the resistance values were determined experimentally. Therefore, the tube and flowmeter resistances were combined into one value (R_{sys}). The resistance of the valve array, since it changes with duty cycle of the PWM wave, is expressed as

$$R_{\text{array}} = \frac{R_{\text{array,open}}}{1 - \text{DC}} \quad (4)$$

where DC is the duty cycle of the PWM signal and $R_{\text{array,open}}$ is the resistance of the valve array when all valves are open (measured experimentally as the inverse of the slope of the flow versus pressure curve, like those shown in Fig. 4, but for the entire 61 valve array). This expression ensures that the total valve

resistance will be equal to $R_{\text{array,open}}$ at 0% duty cycle, and infinity at 100% duty cycle.

The individual inertance components cannot be determined empirically, so they were combined into one value, L_{sys}, and approximated using the equation for fluid inertia through a constant-area pipe segment [5]

$$L_{\text{sys}} = \frac{\rho \ell}{A} \tag{5}$$

where ρ is the fluid density, ℓ is the pipe length, and A is the pipe area.

The final form of the fluidic model equation is therefore

$$P_{\text{reg}} = \left(R_{\text{sys}} + \frac{R_{\text{array,open}}}{1 - \text{DC}} \right) Q + L_{\text{sys}} \dot{Q}. \tag{6}$$

B. Duty Cycle Adjustment

The high linearity of the PWM scheme relies on an ideal square wave for actuation. In practice, however, it is difficult to generate a perfect square wave, given the capacitive nature of the microvalves. Instead, the input square wave consists of finite rise and fall times. This system limitation, along with the mechanical dynamics of the valves, results in a duty cycle that differs slightly from the ideal. The actual duty cycle can be more accurately modeled by including the valve actuation and release times. Specifically

$$\text{DC}_{\text{actual}} = \text{DC}_{\text{ideal}} - f_{\text{PWM}}(t_{\text{act}} - t_{\text{rel}}) \tag{7}$$

where t_{act} and t_{rel} are the valve actuation and release times, respectively, and f_{PWM} is the frequency of the PWM wave. This analysis assumes that the flow rate through a valve is constant until the valve is completely actuated or released. In practice, however, the flow rate changes with the deflection of the plate.

A more accurate version of the fluidic model from the previous section can be obtained by substituting (7) into (6), yielding

$$P_{\text{reg}} = \left\{ R_{\text{sys}} + \frac{R_{\text{array,open}}}{1 - [\text{DC}_{\text{ideal}} - f_{\text{PWM}}(t_{\text{act}} - t_{\text{rel}})]} \right\} Q + L_{\text{sys}} \dot{Q}. \tag{8}$$

C. Open- and Closed-Loop Solution

Obtaining a solution to the system model involves combining the various components: the fluidic model, the time response of the flowmeter, and the dynamic response of the valves (represented by the duty cycle correction previously discussed). With respect to the output (Q) and input $(\text{DC}_{\text{ideal}})$, the fluidic model described above is a nonlinear differential equation. A numerical solution was developed using Simulink, a MATLAB software package for modeling, simulating, and analyzing dynamical systems. Both the open- and closed-loop behaviors of the flow control system were examined.

Simulink allows systems to be drawn in block diagram form. The primary component of the flow control system is the fluidic model (the "plant"), represented by (8). Fig. 11(a) shows this model in Simulink form. The block "DC Frequency Adjustment" adjusts the input duty cycle in accordance with the valve response time.

The fluidic model was integrated into the open-loop system as shown in Fig. 11(b). The input to the system is a step change in open-loop setpoint. (In this context, setpoint is defined as 100% minus the duty cycle.) After being converted to duty cycle, the input signal enters the fluidic model, where the predicted flow rate (Q) is calculated. The triangular block at the output represents a gain factor for unit conversion. Two sets of data are recorded: one directly from the plant and another affected by the delay of the flowmeter. The flowmeter is modeled as a first-order system with a transfer function of the form

$$\text{TF}_{\text{FM}} = \frac{1}{\tau_{\text{FM}} s + 1} \tag{9}$$

where τ_{FM} is the time constant of the flowmeter (measured experimentally).

The block diagram of the closed-loop control system is illustrated in Fig. 11(c). In this case, the input is a step change in target flow rate. After being converted to base units, the system feedback is subtracted and the result enters the block which implements the control algorithm. A proportional-integral (PI) control model is used [6], which is defined by

$$u(t) = K_p e(t) + K_i \int_0^t e(t)\, dt \tag{10}$$

where K_p and K_i are the controller proportional and integral gains, respectively.

The transfer function of the PI control model is given by

$$\frac{U(s)}{E(s)} = K_p \left(1 + \frac{K_i}{s} \right). \tag{11}$$

Before entering the fluidic model, the output from the PI controller passes through the actuator. This block is a means of translating the controller output, in units of flow rate, to a corresponding duty cycle. This is accomplished by manipulating the steady-state form of (8),

$$P_{\text{reg}} = \left\{ R_{\text{sys}} + \frac{R_{\text{array,open}}}{1 - \text{DC}} \right\} Q_{SS}$$
$$\text{DC} = 1 + \frac{Q_{SS} R_{\text{array,open}}}{Q_{SS} R_{\text{sys}} - P_{\text{reg}}}. \tag{12}$$

The output from the plant is recorded and fed back to the summing junction through the flowmeter. As with the open-loop system, both the direct and flowmeter-affected outputs are recorded (controller output versus controller feedback).

IV. System Testing and Results

The completed MFC was tested and the performance results compared to values predicted by the system model. Obtaining accurate results from this model required the determination of a number of system parameters, including the resistance and inertance constants of the fluidic model and the response time of the flowmeter.

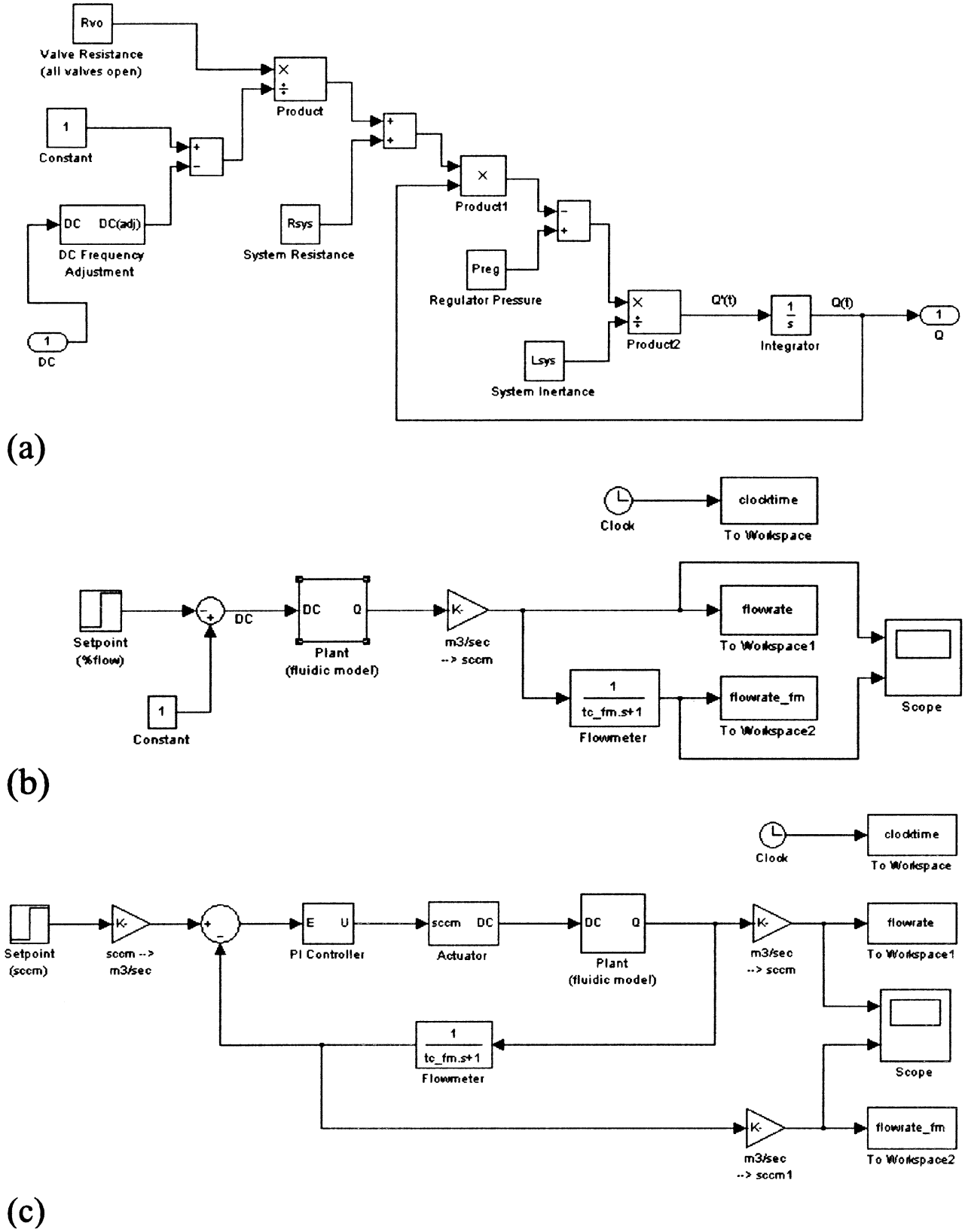

Fig. 11. Simulink representation of flow control system. (a) Fluidic model. (b) Open-loop block diagram. (c) Closed-loop block diagram.

A. Fluidic Model Constants

Numerical solution of the fluidic model developed previously requires the use of three flow parameters: the system resistance (R_{sys}), the valve resistance $(R_{\mathrm{array,open}})$, and the system inertance (L_{sys}). The two resistance values were found empirically using pressure versus flow rate data measured in two situations: with no valve in the system (R_{sys}), and with a DC-400 valve

array mounted in the clamp $(R_{\text{array,open}} + R_{\text{sys}})$. The required resistance values were then found from the slope of the pressure versus flow rate curves to be

$$R_{\text{sys}} = 4.5 \times 10^8 \text{ Pa/m}^3\text{/s}$$
$$R_{\text{array,open}} = (R_{\text{array,open}} + R_{\text{sys}}) - R_{\text{sys}} = 1.379 \times 10^{10} \text{ Pa/m}^3\text{/s}.$$

Note that the system resistance is much smaller than the valve resistance. This is the expected result, due to the extremely small flow area of the microvalves.

The system inertance cannot feasibly be determined through experiment, and was therefore approximated using (5). For a tube diameter of $3/16$ in., a tube length of 31.5 cm, and a gas density of 1.23 kg/m^3, the system inertance was calculated to be

$$L_{\text{sys}} = 21\,750 \text{ kg/m}^4.$$

Note that this analysis treated the distance from the system inlet to the outlet as one constant-area tube. This is an approximation, but should be acceptable for the purpose of estimating the fluidic response time and how it compares to other time constants in the system.

B. Flowmeter Characterization

A number of tests were conducted on the Honeywell AWM3150V mass airflow sensor to analyze its performance. The most important investigation was the empirical determination of the flowmeter time constant. Fig. 12 displays the flowmeter response curves resulting from the sudden opening and closing of a control valve. Of particular interest is the slight increase in flow rate around 0.22 s in Fig. 12(a). This is possibly due to the much slower response time of the mechanical pressure regulator, which is located upstream of the flowmeter.

The time constant of the flowmeter was measured by fitting a curve of the form

$$f(t) = Q_f - (Q_f - Q_i)e^{(-t/\tau_{\text{FM}})} \tag{13}$$

to the data in Fig. 12, where τ_{FM} is the time constant of the response [6] and Q_i is the initial flow rate and and Q_f is the final steady state flow rate. This value was found to be 11 ms for the rising response in Fig. 12(a) and 15 ms for the falling response in Fig. 12(b). Because the overall system cannot respond faster than the slowest time constant, the value of 15 ms was chosen to be used in the open- and closed-loop system models.

Another test performed on the flowmeter involved determination of the optimal PWM frequency used to actuate the valves. At low actuation frequencies, where the period of the PWM wave is much larger than the time constant of the flowmeter, the output signal from the flowmeter is similar in shape to the actuation square wave. This fluctuation is undesirable, since it would require the controller to calculate an average of the signal (at the expense of speed). However, as the PWM actuation frequency increases, the flowmeter cannot respond completely and the peak-to-peak fluctuation in flow rate begins to decrease. Fig. 13 displays the relationship between the amplitude fluctuation of the flowmeter output signal and the PWM valve actuation frequency. Ideally, the time constant of the flowmeter should be much greater than the period of the PWM actuation

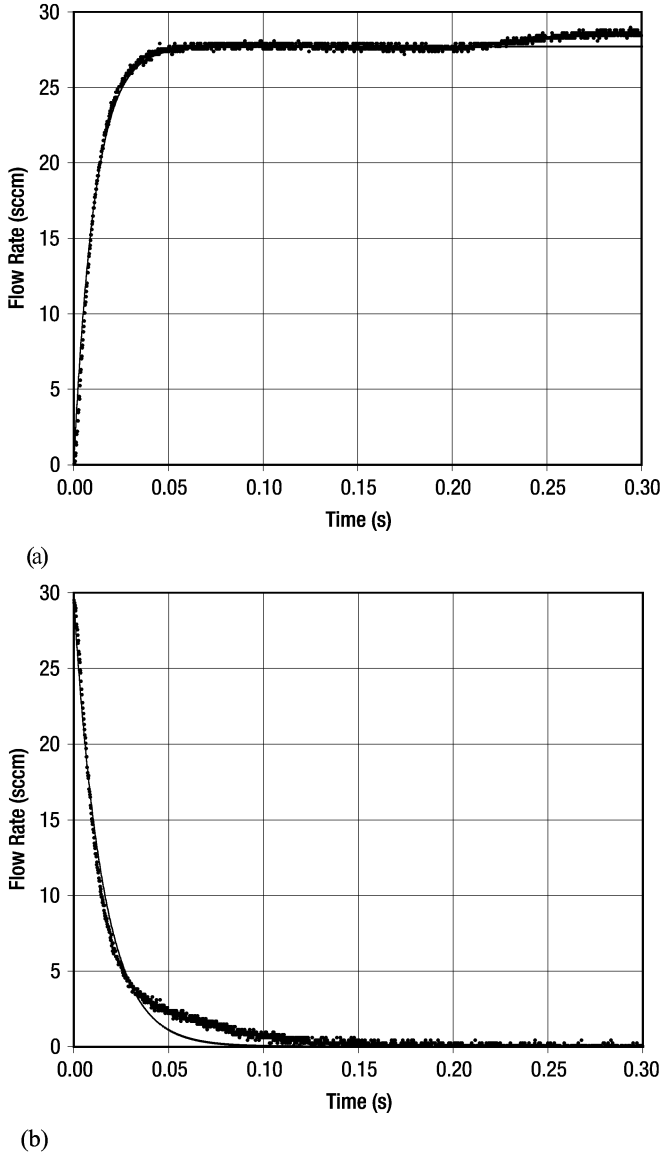

Fig. 12. Response curves of Honeywell AWM3150V flowmeter, with upstream pressure of 1 psi. (a) Valve suddenly opened. (b) Valve suddenly closed. The black lines represent exponential curve fits to the data.

of the valve, but much smaller than the desired time response of the system. To approximate this situation, it was necessary to choose the lowest actuation frequency that minimized fluctuations in the output signal. (Higher frequencies reduce the resolution of the controller.) Therefore, 1000 Hz was chosen as the PWM frequency to be used in system tests of the MFC. Note that oscillations in the flowmeter signal at this frequency were still significant enough to require averaging by the controller, but the averaging time was minimized ($\sim$15 ms).

This shows that the response times for closed loop control using PWM will be several orders of magnitude larger than the valve response times, because of the requirement that the period of the modulation must be much longer than that of the valve response time, but much smaller than the desired system response time (to eliminate oscillations in the sensor output used for feedback). The unique feature of this system is the high-speed microvalves that make fast closed loop response possible.

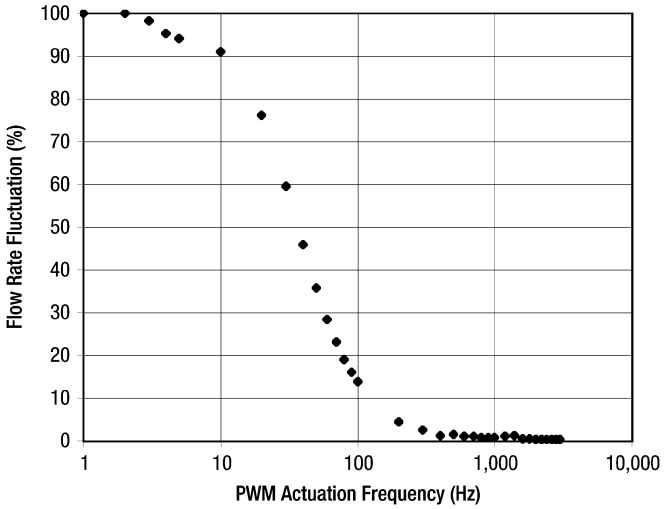

Fig. 13. Peak-to-peak fluctuation of flowmeter output amplitude (expressed as percentage of full-scale flow rate) versus PWM actuation frequency. DC-500 array at 1 psi.

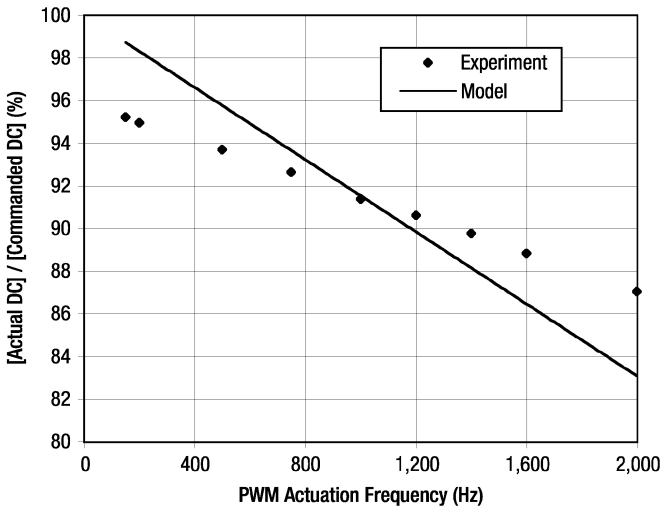

Fig. 14. Variation of actual duty cycle with PWM actuation frequency. Expressed as the ratio of actual duty cycle to commanded duty cycle (50%). DC-500 array at 1 psi.

C. Duty Cycle Analysis

The duty cycle correction discussed in Section III-B was investigated using the mechanical response values found in Section II-A. These actuation and release times were substituted into (7), producing the graph in Fig. 14. This plot compares the predicted duty cycle with actual results for varying PWM actuation frequencies. Note that the results are normalized by the input duty cycle (50%). It is interesting to note that the duty cycle correction model provides the most accurate results around the PWM actuation frequency chosen for system testing (1000 Hz). Fig. 15 displays the relation between flow rate and duty cycle at an actuation frequency of 1000 Hz, comparing the model correction to experimental results.

The nonlinearities near the extreme ends of the flow rate versus duty cycle graph in Fig. 15 prompted the determination of the duty cycle range which could be expected to provide a linear relationship between flow rate and duty cycle. The minimum and maximum values of this range were calculated

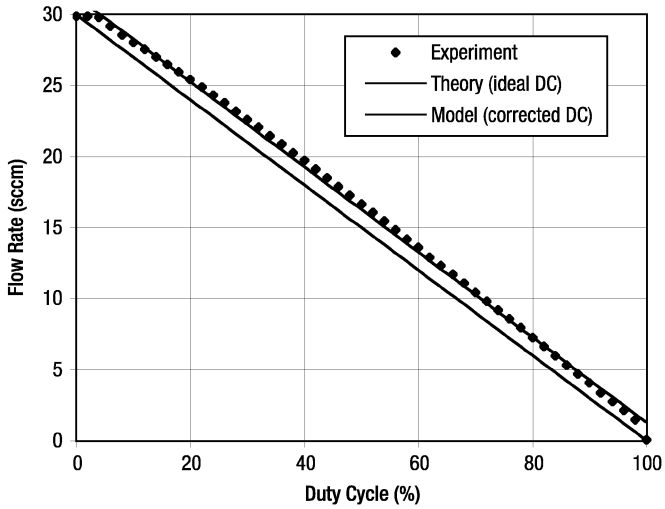

Fig. 15. Comparison of PWM flow results based on ideal and model-corrected duty cycles. PWM actuation frequency is 1000 Hz. DC-500 array at 1 psi.

by substituting $\mathrm{DC}_{\mathrm{ideal}} = 0\%$ and $\mathrm{DC}_{\mathrm{ideal}} = 100\%$ into (7), indicating that the linearity of the PWM actuation method at 1000 Hz is valid over the range

$$4.2\% \leq \mathrm{DC}_{\mathrm{ideal}} \leq 95.8\%$$

which is consistent with the empirical results in Fig. 14.

This range of flow rates corresponds to a dynamic range of about 23:1. The dynamic range value is limited by the 1 kHz modulation frequency (needed for reducing flow meter oscillations) combined with the difference in actuation and release times for the valves. In addition, the 2% leakage rate limits the maximum possible dynamic range to 50:1. Reducing the modulation frequency could improve the dynamic range, but this would likely require longer averaging times to eliminate the increased oscillations in the flow meter output, thus increasing overall response times. This shows that there is a tradeoff between dynamic range and system response time.

An important operating limitation, related to duty cycle, is the resolution of the PWM actuation scheme. In the case of the system developed for this research, the resolution is limited primarily by the speed of the microcontroller. The PWM module of the Motorola HC12 specifies the duty cycle of the output wave in terms of clock cycles. Therefore, the minimum duty cycle change is determined by calculating the length of one clock cycle, and dividing it by the period of the wave. This is expressed by

$$\Delta\mathrm{DC}_{\mathrm{min}} = \frac{(1/f_{\mathrm{MCU}})}{T_{\mathrm{PWM}}} = \frac{f_{\mathrm{PWM}}}{f_{\mathrm{MCU}}} \tag{14}$$

where f_{MCU} is the clock frequency of the microcontroller. For a clock frequency of 8 MHz and a PWM frequency of 1000 Hz, the theoretical minimum duty cycle change was calculated to be 0.0125%.

D. Open-Loop Results

All results described below were obtained for a DC-400 array without dimples at a regulated pressure of 1 psi.

The open-loop response of the controller was investigated theoretically under two conditions: with and without the

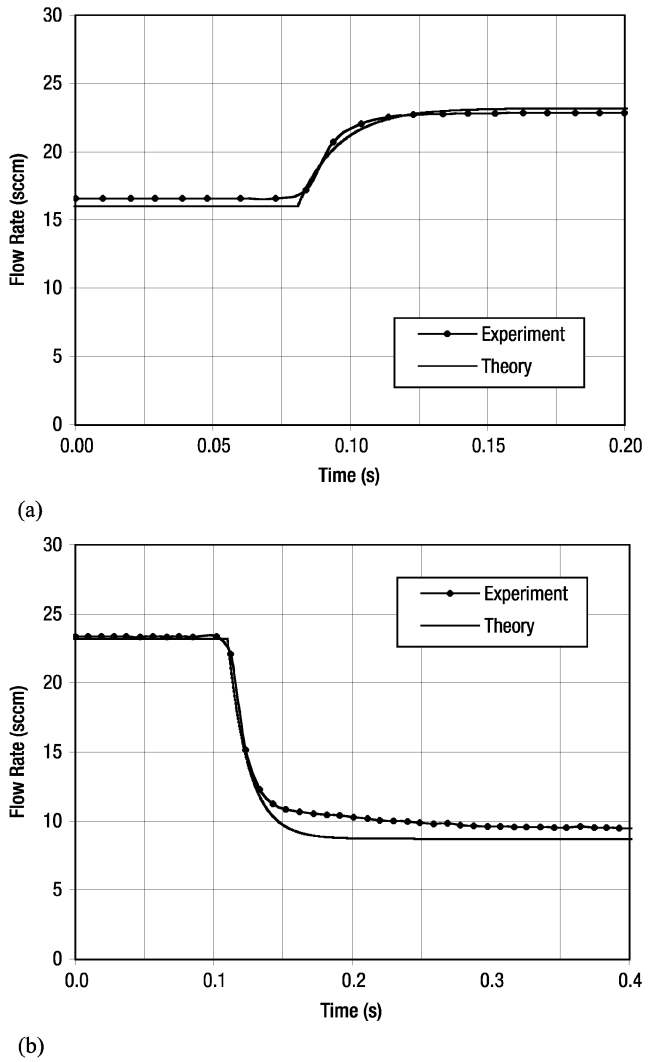

Fig. 16. System response to changes in open-loop setpoint. (a) 50 to 75%. (b) 75 to 25%. Note the difference in time scales.

flowmeter attached to the output. When the flowmeter is neglected, only the fluidic response time is relevant, and the model indicated that this value is on the order of microseconds (1.2 μs). With the flowmeter connected to the system, however, the response is significantly slower. Fig. 16 displays step changes to the open-loop system with the flowmeter attached, comparing the model solution to empirical results. It is evident from these graphs that the open-loop time constant is approximately equal to the flowmeter time constant from Section IV-B, indicating that the overall system response is dominated by the flowmeter.

From a numerical standpoint, the time constant of the flowmeter is approximately 12 500 times larger than that of the fluidic model alone. This suggests that the fluidic model may be ignored when simulating the system dynamics. Note that this statement is based on results obtained using a simple model for system inertance (5). However, the time constant associated with this inertance is four orders of magnitude smaller than flowmeter time constant; this difference is most likely well outside any uncertainty associated with the inertance value.

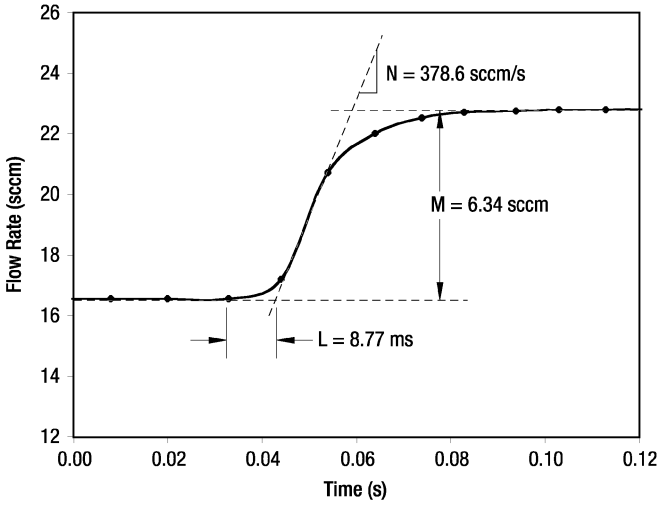

Fig. 17. Ziegler-Nichols method applied to open-loop response (step change in setpoint from 50 to 75%).

E. Closed-Loop Results

Optimizing the performance of the closed-loop control system required careful selection of the proportional and integral gain values. For this paper, the Ziegler-Nichols method [7] was employed, which uses characteristics of the open-loop response to predict optimal closed-loop gain values. For a proportional-integral control model, the Ziegler-Nichols gains are specified as

$$K_p = 0.9\frac{M}{\mathrm{NL}} \tag{15}$$

$$K_i = 0.3\frac{M}{\mathrm{NL}^2} \tag{16}$$

where M, N, and L are measured from the empirical open-loop response, as shown in Fig. 17. The final gain values were calculated to be

$$K_p = 1.72$$
$$K_i = 65.3.$$

These values were programmed into both the Simulink closed-loop model and the controller onboard the MFC. The discretized control model used by the MFC is given by

$$u_n = u_{n-1} + K_p(e_n - e_{n-1}) + K_i\Delta t(e_n) \tag{17}$$

where Δt is the discrete sampling interval used by the MFC. The MFC can operate in remote interface mode, with LabVIEW used as an interface for control inputs and data acquisition. In this mode, LabView limited the value of Δt to 10 ms. Use of smaller values for Δt would not provide improved performance, since the flow meter time constant (15 ms) is the limiting time scale for the control.

The response curves of the closed-loop control model are compared to the actual MFC response in Fig. 18. Fig. 19 displays the closed-loop performance of the MFC over a 12-s time period, as it responds to various changes in flow rate setpoint. The gains calculated by the Ziegler-Nichols method provided a relatively quick response, with a time constant of approximately 25 ms. The graphs indicate that the Simulink model predicts

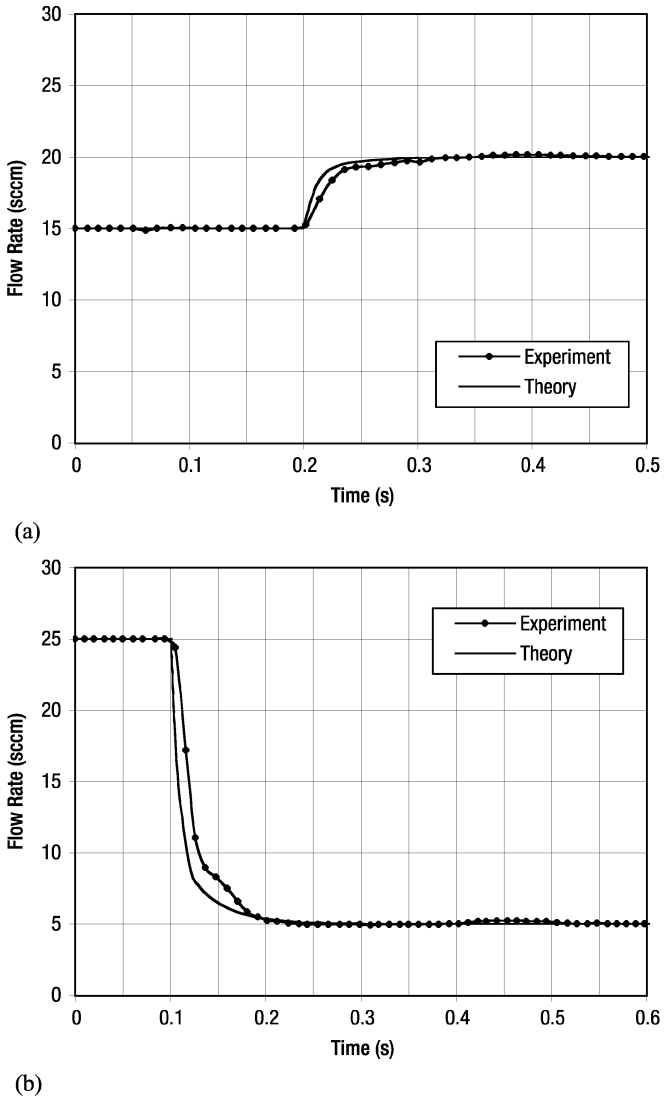

Fig. 18. Closed-loop response of flow control system. (a) 15 to 25 sccm step change. (b) 25 to 5 sccm.

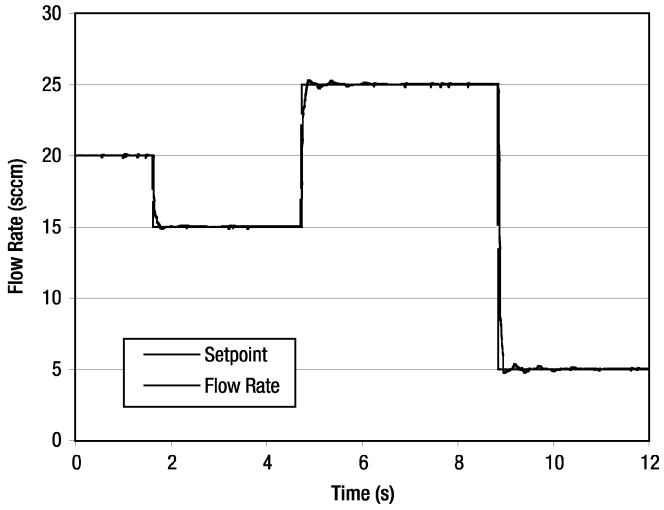

Fig. 19. MFC closed-loop response to various changes in flow rate setpoint.

the closed-loop response of the MFC system with considerable accuracy.

The response of the MFC is significantly better than the Redwood MicroSystems MEMS-Flow™ mass flow controller, which also is based on a MEMS microvalve. MEMS-Flow™ has a response time of 1.5 s to 2% of the setpoint [8]. Based on a 25-ms time constant, the response time of this MFC is about 100 ms to 2% of setpoint, an order of magnitude faster. MEMS-Flow™ does have a larger dynamic range, 50:1- a value that may be possible with this MFC if leakage effects could be reduced.

V. Conclusion

This paper documented the evaluation of MEMS microvalve arrays through the development of a compact, stand-alone MFC. The microvalve array consists of polysilicon plates anchored over holes in a silicon substrate. The individual valves are closed using electrostatic actuation; applying a voltage to the plate causes it to snap shut over the corresponding hole. Prior to the construction of the MFC, a number of experiments were conducted to evaluate the operating characteristics of the microvalves and determine if a particular valve design was more suited for use with the device. Additionally, a mathematical representation of the system was developed to model the dynamic performance of the MFC.

Experiments conducted on the microvalves indicated that the double-cantilever design, in 400 and 500 μm sizes, would provide the best performance for the flow control system; this was due to its good flow rate versus pressure characteristics, low leakage rate, and resistance to stiction. Other tests conducted on the valves included reverse flow and leakage experiments, as well as mechanical response measurements.

To use the valves effectively for flow control, a PWM technique was used. This technique, which involves actuating the microvalves with a high frequency square wave and varying the duty cycle to regulate flow rate, was found to be superior to other actuation schemes due to its higher resolution and simplicity. The use of PWM in fluid control is not a new idea. The unique aspect of this paper is the combination of PWM with high speed MEMS μvalves and closed loop mass flow control to create a rapid response MFC with high resolution and good dynamic range.

These features were demonstrated through a series of experiments that showed a system time constant of approximately 25 ms for response to changes in setpoint, a value predicted quite accurately by a mathematical model.

Since flow rate is dependent on the duty cycle of the actuation signal, the resolution of the system is reliant primarily on the speed and quality of the driving electronics, not the microvalves themselves. The system developed for this research contained an 8-MHz microcontroller, which resulted in a minimum duty cycle adjustment of 0.0125%. (This corresponds to approximately 0.004 sccm at 1 psi.)

Another goal of the flow control system, scalability, is related to this resolution issue. The valve arrays fabricated for this research were comprised of only 61 microvalves, but much larger arrays could be manufactured to handle wider flow ranges. Increasing the range of a flow control device traditionally decreases its resolution, but with the gigahertz microprocessors

available today, the PWM actuation technique would allow high resolution flow control even with larger flow rate ranges.

The primary obstacle to scalability and dynamic range, regardless of the actuation method, is valve leakage. At an operating pressure of 1 psi, leakage through a 61-element array was found to be approximately 2% of the full-scale flow rate. Increasing the number of microvalves in the array would cause the overall leakage to increase as well. This problem could be countered by redesigning the dimples on the valve plate, which serve to aid sealing during actuation.

REFERENCES

[1] N. Vandelli, "Development of MEMS micro-valve arrays for fluid flow control," Ph.D. dissertation, Boston Univ., MA, 1999.
[2] N. Vandelli, T. G. Bifano, D. Wroblewski, and M. Velonis, "Development of a MEMS micro-valve array for fluid flow," *J. Microelectromech. Syst.*, vol. 7, pp. 395–403, Dec. 1998.
[3] C. Hodge, "The Evaluation of MEMS microvalve arrays for fluidic control," M.S. thesis, Boston Univ., MA, 2000.
[4] C. Hodge, D. Wroblewski, and T. G. Bifano, "Evaluation of MEMS microvalve arrays as fluid controllers," in *Proc. ASME Fluids Engineering Division Summer Meeting*, 2000.
[5] R. R. Rosenberg, *Introduction to Physical Systems Dynamics*. New York: McGraw-Hill, 1983.
[6] K. Ogata, *Modern Control Engineering*. Englewood Cliffs, NJ: Prentice-Hall, 1990.
[7] T. G. Bifano, "Implementing a PID controller for PZT actuation," Boston Univ., MA, unpublished report, 1992.
[8] MEMS-Flow™ Gas MFC, Product Specifications [Online]. Available: www.redwoodmicro.com/Datasheets/GMFC1-2w.pdf

John Collier received the B.S. degree in mechanical engineering from Rose-Hulman Institute of Technology, Terre Haute, IN, in 1999, and the M.S. degree in mechanical engineering from Boston University, Boston, MA, in 2002.

From 2000 to 2002, he was a Graduate Research Assistant with the Precision Engineering Research Lab, Boston University, where he worked closely with the Boston Micromachines Corporation. His work was focused on developing control systems for MEMS fluidic valves.

Donald Wroblewski received the B.S. degree in mechanical engineering from Pennsylvania State University, University Park, and the M.S. and Ph.D. degrees from the University of California, Berkeley.

He is an Associate Professor with the Aerospace and Mechanical Engineering Department, Boston University, Boston, MA. His background encompasses more than 20 years of experience in thermal-fluids research, including eight years in industry and consulting and 13 years in academic research. His research areas include design and characterization of MEMS microvalve arrays, modeling and experimental studies of plasma spray processes, and evaluations of aircraft measurements of atmospheric turbulence.

Thomas Bifano received the B.S. and M.S. degrees in mechanical engineering from Duke University, Durham, NC, and the Ph.D. degree in mechanical engineering from North Carolina State University, Raleigh.

He is a Professor and Chair of the Manufacturing Engineering Department, Boston University, Boston, MA, with a joint appointment as a Professor in the Aerospace and Mechanical Engineering Department. His research focuses on development of microelectromechanical systems (MEMS) for optical and biomedical applications. He joined Boston University, Boston, MA, in 1988. He is a founding faculty member of the Boston University Photonics Center, and a faculty member of the Fraunhofer Center for Manufacturing Innovation. He is also Chief Technology Officer for Boston Micromachines Corporation.